ACS Chemical Neuroscience

pubs.acs.org/chemneuro

Research Article

Photoswitchable ORG25543 Congener Enables Optical Control of Glycine Transporter 2

Shannon N. Mostyn,[‖] Subhodeep Sarker,[‖] Parthasarathy Muthuraman, Arun Raja, Susan Shimmon, Tristan Rawling, Christopher L. Cioffi, and Robert J. Vandenberg*

Cite This: *ACS Chem. Neurosci.* 2020, 11, 1250−1258

Read Online

ACCESS | Metrics & More | Article Recommendations

ABSTRACT: Glycine neurotransmission in the dorsal horn of the spinal cord plays a key role in regulating nociceptive signaling, but in chronic pain states reduced glycine neurotransmission is associated with the development of allodynia and hypersensitivity to painful stimuli. This suggests that restoration of glycine neurotransmission may be therapeutic for the treatment of chronic pain. Glycine transporter 2 inhibitors have been demonstrated to enhance glycine neurotransmission and provide relief from allodynia in rodent models of chronic pain. In recent years, photoswitchable compounds have been developed to provide the possibility of controlling the activity of target proteins using light. In this study we have developed a photoswitchable noncompetitive inhibitor of glycine transporter 2 that has different affinities for the transporter at 365 nm compared to 470 nm light.

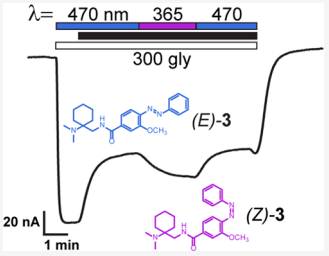

KEYWORDS: *Glycine transport, glycine transporter 2 inhibitor, photoswitchable inhibitor, ORG25543 congener, chronic pain, neuropathic pain*

INTRODUCTION

Chronic neuropathic pain is a debilitating disease, which arises as a result of nerve damage and rewiring of circuits within the pain processing pathway.[1] One of the major changes to the central nervous system during this process is an emerging predominance of excitatory tone in the spinal cord dorsal horn.[2] Under normal nociception, excitatory glutamatergic neurons are controlled by a subpopulation of inhibitory glycinergic neurons in the dorsal horn.[3] It has been shown in a rodent model of neuropathic pain that these inhibitory projections to radial neurons are diminished.[4] Therefore, a loss of inhibitory inputs would allow for unregulated nerve firing in the ascending pain pathway, producing the battering of enhanced pain sensations characteristic of chronic pain.

Glycine concentrations within inhibitory synapses are tightly controlled by the glycine transporter, GlyT2,[5] and may therefore be a promising target for therapeutics which would act to restore normal nociceptive control.[6−9] Indeed, knockdown of GlyT2 via targeting siRNA to ∼30% expression produces analgesia in rat models of pain.[10] While partial knockdown of GlyT2 produces analgesia with no observable behavioral side effects, total gene knockout of GlyT2 in mice produces severe neuromotor symptoms, with death 2 weeks postnatal.[11] Additionally, electrophysiological recordings from knockout GlyT2 mice show a reduction of postsynaptic glycinergic currents, which highlights the important role of GlyT2 for recycling of glycine into presynaptic vesicles. The GlyT2 knockout phenotype shows similarities with hyperekplexia, a severe neuromotor disease where strong tremor can be induced through touch, and subjects experience muscle rigidity and an inability to right themselves. Mutation of the human gene encoding GlyT2 (*SLC6A5*) is the most common presynaptic cause of hyperekplexia, with mutations altering glycine and/or ion binding sites, as well as affecting localization and expression in the plasma cell membrane.[12−15]

ORG25543 (**1**) (Figure 1) is a GlyT2 inhibitor that ameliorates both hallmarks of neuropathic pain: hyperalgesia, the heightened pain response, and allodynia, an improper response to innocuous stimuli.[10,15] Unfortunately, acute dosing in rodents produces excitotoxicity, hyperekplexia-like symptoms, and in severe cases death.[16,17] Exposure of mouse spinal cord slices to ORG25543 for >10 min results in a long-term reduction of inhibitory postsynaptic currents,[18] likely to be due to blockade of glycine recycling. Furthermore, glycinergic currents cannot be restored following washout of ORG25543 from oocytes expressing GlyT2,[16] suggesting sustained, complete block of glycine transporters mimics the GlyT2 knockout phenotype. Following the abandonment of many GlyT2 inhibitor programs, Mingorance-Le Meur, Courade, and colleagues resurrected the ORG25543 scaffold and produced a series of analogues to examine the requirements for on-target

Received: December 8, 2019
Accepted: March 19, 2020
Published: March 19, 2020

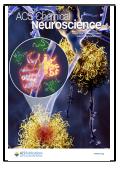

https://dx.doi.org/10.1021/acschemneuro.9b00655
ACS Chem. Neurosci. 2020, 11, 1250−1258

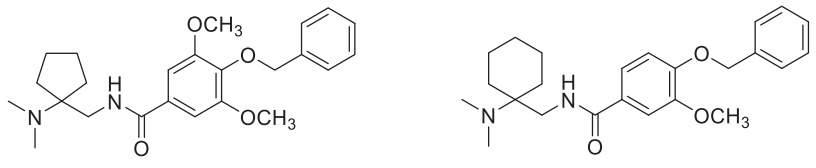

Figure 1. Structures of the reported GlyT2 inhibitors ORG25543 (**1**) and compound **2**.

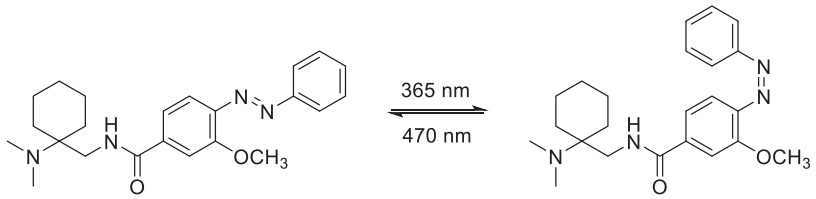

Figure 2. Geometric isomers of photochromic azobenzene **3**, (*E*)-**3** and (*Z*)-**3**. Compound **3** interconverts between the more thermodynamically stable (*E*)-**3** (*trans*) isomer and the less stable (*Z*)-**3** (*cis*) isomer upon irradiation of λ = 365 nm or λ = 470 nm light.

toxicity.[16] Analogue **2** is one such compound with an IC_{50} at GlyT2 of 100 nM but importantly allows for restoration of glycine currents following its reversible binding. Compound **2** is blood brain barrier permeable, produced analgesia in rodent models of neuropathic pain, and displayed no adverse side effects. It is therefore predicted that GlyT2 inhibitors should be reversible to allow for recycling of glycine, which should circumvent toxicity while maintaining analgesic activity. In order for ORG25543-based GlyT2 inhibitors to be further developed, greater insight into the mechanism of reversible binding and their effects on glycinergic neurotransmission should be obtained.

The emerging field of photopharmacology allows for spatiotemporal control of cellular activity using light-sensitive chemical compounds, whereby incorporation of a photosensitive moiety into a desired chemical structure produces active compounds that possess a switch that can be precision controlled using certain light wavelengths.[19] These light controllable compounds are powerful tools for noninvasive manipulation and monitoring of cellular activity in living cells and organisms.[20] The azobenzene moiety is one of the most widely used photoswitches, where incorporation produces a molecule that can undergo *cis*-to-*trans* isomerization around the diazo N═N bond upon irradiation with UV or blue visible light[21] (Figure 2). Azobenzenes are metabolically stable, undergo rapid *trans*-to-*cis* isomerization, and thermally relax back to the thermodynamically more stable *trans* geometric isomer from between milliseconds to days depending on the electronic properties of the azobenzene substituents and the temperature and ionic strength of the solvent. Because of their desirable properties, azobenzene photoswitchable compounds have been successfully used to study proteins involved in rapid synaptic transmission, such as ion channels and transporters.[22−24] The GlyT2 inhibitor **2** is well suited to azologization because it contains a benzyl phenyl ether moiety that is structurally homologous to azobenzenes in the *trans* configuration.[25] In this study we have produced the photochromic azobenzene **3** that was derived from direct azologization of GlyT2 inhibitor **2** (Figure 2). Azobenzene **3** readily photoswitches between the *Z* and *E* geometric isomers upon irradiation with λ = 365 nm or λ = 470 nm light. We examined the inhibitory activity of both geometric isomers (*E*)-**3** and (*Z*)-**3** at GlyT2 and investigated their reversibility and mechanisms of inhibition.

RESULTS AND DISCUSSION

Chemistry. The synthesis of diazo photochromic compound **3** begins with the preparation of 1-(aminomethyl)-*N*,*N*-dimethylcyclohexan-1-amine (**6**), which is presented in Scheme 1. Amino nitrile **5** was manufactured via a Strecker

Scheme 1[a]

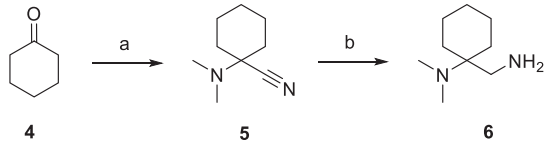

[a]Reagents and conditions: (a) dimethylamine hydrochloride, KCN, H_2O, rt 16 h; (b), $LiAlH_4$, Et_2O, 0 °C to rt, 18 h.

condensation reaction between cyclopentanone (**4**) and dimethylamine hydrochloride in the presence of KCN. Nitrile **5** was subsequently reduced to diamine **6** using $LiAlH_4$. The high volatility of **6** prohibited *in vacuo* concentration and isolation of it upon extraction into Et_2O during the workup. Therefore, crude **6** was used in the subsequent peptide coupling reaction as a solution in Et_2O, with an estimated concentration of ∼0.49 M as per the theoretical yield for the $LiAlH_4$ reduction.

The next phase of the synthesis of azo-compound **3** is shown in Scheme 2. Aniline **7** underwent a Baeyer-Mills coupling reaction with commercially available nitrosobenzene in HOAc at 40 °C to afford (*E*)-**8**. Only one product was observed for this reaction by LC-MS (data not shown) and ^{1}H NMR analysis, which was presumed to be the more thermodynamically stable *trans* geometric isomer (*E*)-**8**. Saponification of the methyl ester of (*E*)-**8** with 2 M NaOH gave the corresponding carboxylic acid (*E*)-**9**, which underwent a subsequent peptide coupling reaction with previously described amine **6** in the presence of HBTU and *i*-Pr_2NEt in THF. This reaction produced photochromic compound **3** as an orange solid, which

https://dx.doi.org/10.1021/acschemneuro.9b00655
ACS Chem. Neurosci. 2020, 11, 1250−1258

Scheme 2[a]

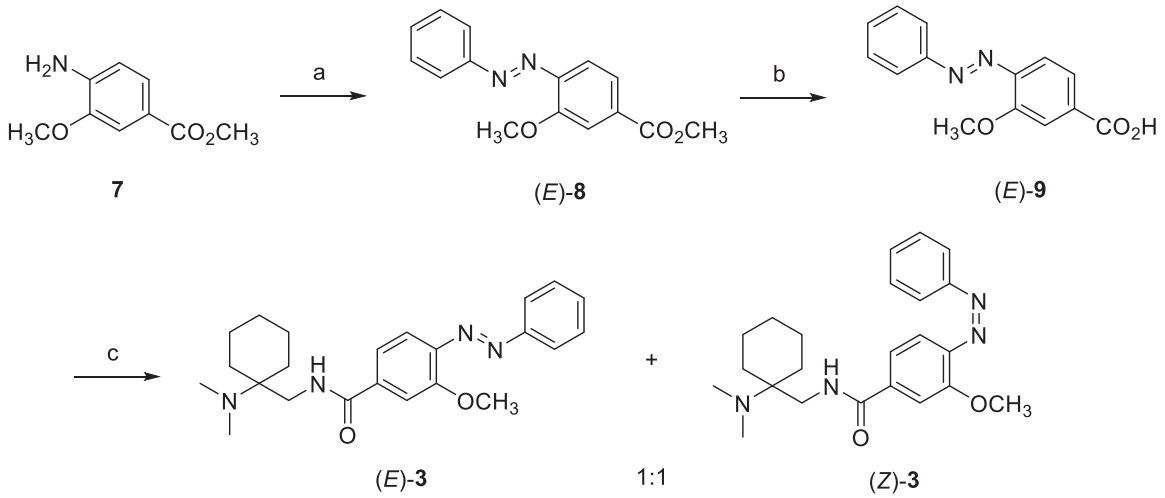

[a]Reagents and conditions: (a) nitrosobenzene, HOAc, 40 °C, 48 h; (b) aqueous 2 M NaOH, CH_3OH, THF, rt, 16 h; (c) **6**, HBTU, *i*-Pr_2NEt, THF, 0 °C to rt, 16 h.

was found to be a ∼1:1 mixture of *E* and *Z* isomers. Repeated attempts to isolate and independently characterize (*E*)-**3** and (*Z*)-**3** were deemed futile as both geometric isomers quickly interconverted upon purification and in the presence of visible light to give a nearly 1:1 mixture of both compounds. The LC-MS, HPLC, and ^{1}H NMR data confirmed that compound **3** is a mixture that contains only (*E*)-**3** and (*Z*)-**3**, and the HPLC data indicates an overall purity for **3** to be at 99.76%.

Azo-Compound 3 Is Photoswitchable. The photoswitchable properties of azo-compound **3** in solution were investigated using UV/vis spectroscopy. Phosphate-buffered saline (PBS) buffered to pH 7.4 was used as the solvent to reflect the conditions of the GlyT2 inhibition assay. The UV−vis spectrum of a solution of **3** preirradiated with 470 nm light displayed a strong UV absorption band at 316 nm and a weaker band at ∼430 nm (Figure 3A, blue line). These absorptions arise from $\pi-\pi^*$ and $n-\pi^*$ transitions in *trans*-azobenzenes, respectively,[21] and confirm the presence of (*E*)-**3** in the solution. Irradiation of the sample with 365 nm UV light produced a change in the UV/vis spectrum toward an absorption profile characteristic of *cis*-azobenzenes (Figure 3A, purple line). Thus, the strong band at 316 nm was replaced with a weaker absorption band at 290 nm which arises from $\pi-\pi^*$ transition in (*Z*)-**3**. Subsequent irradiation of the solution with 470 nm blue light caused the UV/vis spectrum to return to that of the *trans*-azobenzene (*E*)-**3** (Figure 3A, blue line). We also studied the thermal relaxation of (*Z*)-**3** because *cis*-azobenzenes thermally isomerize to their more stable *trans* configuration in the absence of light. A solution of (*Z*)-**3**, formed by preirradiation with 365 nm light, was left in the dark and monitored by UV/vis spectroscopy every 12 h. As shown in Figure 3B, the characteristic *cis*-azobenzene absorption band at 290 nm decreased and was replaced with the 316 nm *trans*-azobenzene absorption band, and complete thermal relaxation to (*E*)-**3** occurred in 84 h. Collectively, these experiments show that azo-compound **3** is readily and reversibly photoswitchable and can be isomerized in real-time biological assays.

Activity of Azo-Compound 3 at GlyT2. Glycine transport by GlyT2 is coupled to the cotransport of 3 Na^+ and 1 Cl^-, which generates an electrogenic process that can be measured using the two-electrode voltage clamp technique with *Xenopus laevis* oocytes expressing GlyT2. Under this experimental design, ORG25543 and analogue **2** have previously been shown to inhibit GlyT2 with potencies of 20 nM and 100 nM, respectively.[16] Inhibition by ORG25543 was irreversible and was maintained for 10 min after cessation of application, while **2** is readily reversible. We first confirmed their actions on GlyT2 by demonstrating a comparable dose dependent reduction of glycine transport currents, with IC_{50} values of 3.76 (2.36−6.01) nM and 48.5 (42.6−55.2) nM (Figure 4A). We also observed restoration of glycine transport currents following reversible binding of **2** but no reversibility of ORG25543, even after 30 min of washout (Figure 4B).

Following validation of the activity of the parent compounds in our assay, compound **2** was chosen as the base compound for generating the photoswitchable analogue, **3**, because of its reversibility. Compound **3** was examined for the ability of each photoswitchable isomer to inhibit GlyT2. An external light source with a liquid light guide was connected to tubes of recording buffer containing **3**, and photoswitching in real-time was achieved by alternating between λ = 365 nm and λ = 470 nm. We began by preirradiating **3** with λ = 470 nm light to ensure **3** remained in its thermally relaxed *trans* configuration state ((*E*)-**3**). Perfusion of GlyT2 expressing oocytes with buffer containing glycine produced inward currents that were blocked by (*E*)-**3** (Figure 5A). Once a steady state of inhibition was reached, the light was switched to λ = 365 nm, and an increase in transport current was observed, indicating GlyT2 was less sensitive to inhibition by the *cis* isomer ((*Z*)-**3**). The light was again switched back to λ = 470 nm, and (*E*)-**3** produced the same level of inhibition compared to the preirradiated analogue, demonstrating real-time isomerization could be achieved in this electrophysiological assay. The recording chamber was then washed for 10 min, and the assay was repeated but beginning with preirradiated (*Z*)-**3**, showing that comparable levels of inhibition are achieved regardless of the order of photoswitching (Figure 5A). Following the inhibitory assay, the oocyte was again washed, and glycine was reapplied to show that currents could be restored. In contrast to **1**, inhibition by **3** is fully reversed after 5 min, and glycine transport currents were restored to

https://dx.doi.org/10.1021/acschemneuro.9b00655
ACS Chem. Neurosci. 2020, 11, 1250−1258

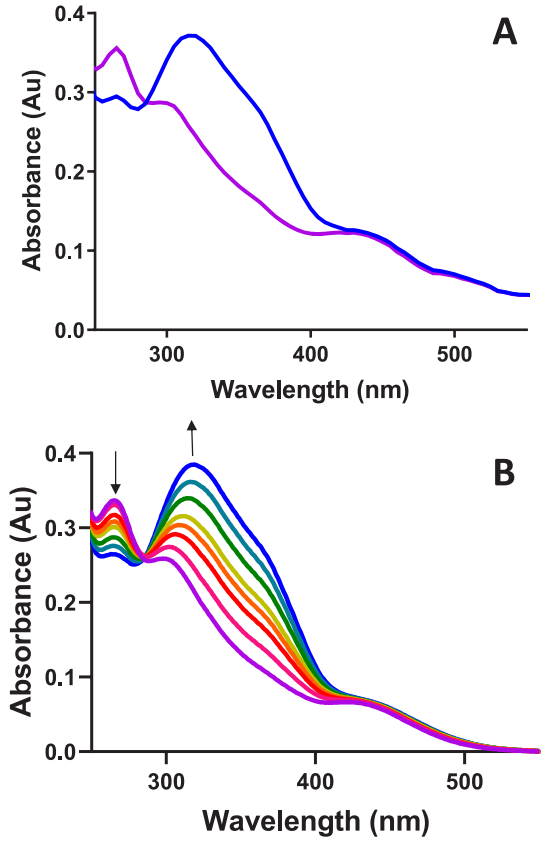

Figure 3. Photoisomerization of azo-compound **3**. **A.** A solution of azo-compound **3** in PBS (pH 7.4) was irradiated with 470 nm blue light for 15 min to ensure **3** was in the *trans* configuration, and the corresponding UV−visible absorption spectrum was measured (blue line). (*E*)-**3** was then irradiated with 365 nm UV-A light in 5 s intervals until no further change in absorbance was observed (purple line), and (*Z*)-**3** was formed. The solution was irradiated with 470 nm light, and (*Z*)-**3** isomerized back to the *trans* isomer ((*E*)-**3**) (blue line). **B.** Thermal relaxation of (*Z*)-**3**. Compound **3** was isomerized to (*Z*)-**3** with 365 nm UV-A light and then allowed to thermally relax to (*E*)-**3** in the dark over an 84 h time period. UV−vis spectra were recorded at 12 h intervals. Complete isomerization to (*E*)-**3** occurred over 84 h.

preinhibition levels (Figure 5C). Compound **3** was also tested on oocytes expressing GlyT1 and was found to have no activity at either 365 or 470 nm (Figure 5B).

To determine the IC_{50} values for each isomer, increasing concentrations of **3** irradiated with either λ = 365 nm or λ = 470 nm light were applied to GlyT2 expressing oocytes to block currents generated by 3, 10, 30, 100, 300, and 1000 μM glycine (Table 1, Figure 5B − representative concentration response curves at 30 μM glycine). The IC_{50} values were consistent at each glycine concentration, and average IC_{50} values were calculated to be 9.94 μM and 5.36 μM for (*Z*)-**3** and (*E*)-**3**, respectively. Both isomers of **3** are active inhibitors of GlyT2, with the *trans* configuration possessing a marginally higher potency than *cis*. While both isomers are active, they are >110-fold less potent than the nonazologized parent analogue, **2**. This observed loss in potency may be attributed to one of the following factors (or any combination thereof): 1) diminished affinity may result from an inability of the azobenzene appendage of (*E*)-**3** or (*Z*)-**3** to adopt a putative bioactive conformation proposed for the benzyl ether appendage of ORG25543[15] due to potential preferred orientations between the adjacent diazo and methyl ether groups,[26,27] 2) the electron withdrawing diazo bridge may also impart unfavorable electronic effects on the pendant phenyl ring,[28] which could lead to a loss in potency due to potentially diminished $\pi-\pi$ stacking or π-cation binding interactions, and 3) the azobenzene group may be projecting into a hydrophobic binding pocket and may not be well-tolerated due to the increased polarity of the diazo bridge relative to the benzyl ether tether of ORG25543 and compound **2**.

In order to determine the mechanism of glycine transport inhibition at GlyT2, glycine concentration response curves were performed in the presence of increasing concentrations of (*Z*)-**3** or (*E*)-**3** (Figure 6A,B, Table 2). EC_{50} values for each concentration of **3** at both λ = 365 and 470 nm are unchanged, while I_{max} decreased as the concentration of **3** increased, which suggests that neither isomer of **3** is competing for the glycine binding site. Additionally, Eadie-Hofstee plots of the data confirm **3** is a noncompetitive inhibitor (Figure 6C,D). Inhibitors of the SLC6 family of transporters usually bind in either the central substrate site and compete for glycine or their binding site lies at a wider point of the transporter cavity in a location referred to as either the "substrate S2" site or "allosteric" site. For the related serotonin transporter, the transport blocker (*s*)-citalopram can bind in either the central substrate site or the allosteric site to inhibit serotonin reuptake.[29] GlyT2 possesses the smallest central substrate site of the SLC6 family and cannot transport any other substrates other than glycine.[30] GlyT2 also has no known

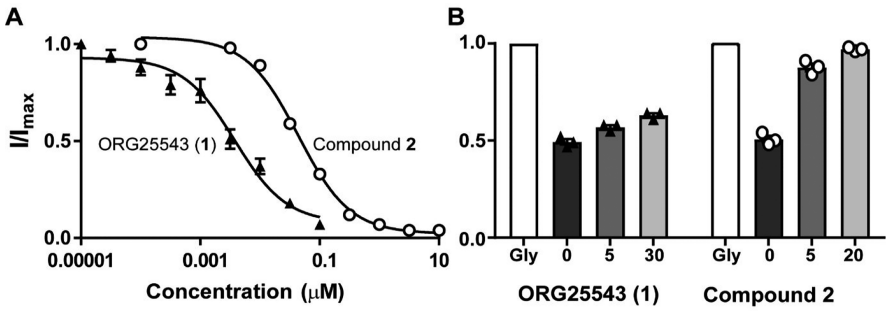

Figure 4. ORG25543 (**1**) and compound **2** inhibit glycine evoked currents. **A.** Increasing concentrations of **1** and **2** were applied to oocytes expressing GlyT2, to reduce glycine transport currents. **B.** Following cessation of inhibition by IC_{50} concentrations of **1** (4 nM) and **2** (50 nM) (time 0), oocytes were washed with ND96 for 30 min, and glycine was reapplied at 5 min intervals to compare currents to preinhibition levels (Gly).

https://dx.doi.org/10.1021/acschemneuro.9b00655
ACS Chem. Neurosci. 2020, 11, 1250−1258

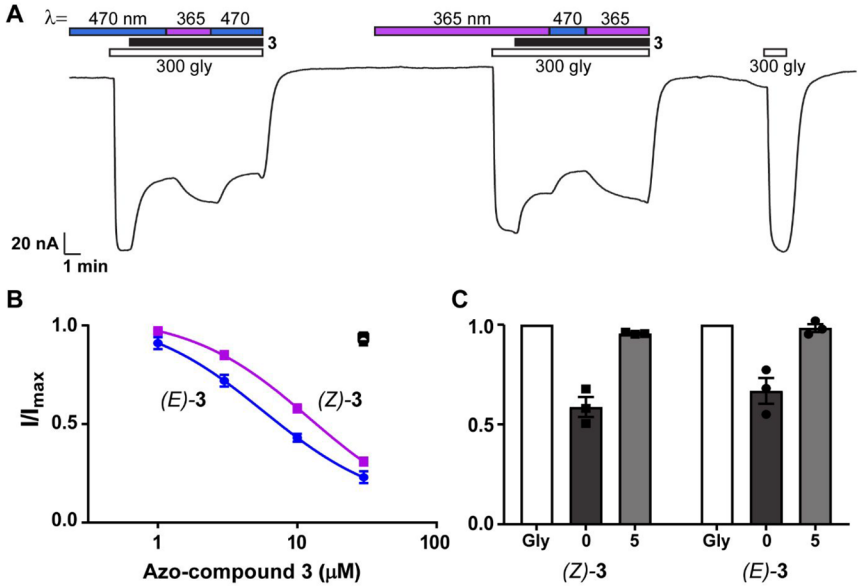

Figure 5. Activity of **3** at GlyT2 expressing oocytes. **A.** Current trace of 10 μM **3** mediated inhibition of 300 μM glycine transport by GlyT2. 300 μM glycine was applied to oocytes expressing GlyT2 to produce an inward current. **3** was irradiated with λ = 470 nm light to preserve the thermally relaxed *trans* state ((*E*)-**3**) and was then coapplied with glycine until stable inhibition was reached. **3** was then immediately irradiated with λ = 365 nm to shift the conformation to *cis* ((*Z*)-**3**), and irradiation was continued until a new stable point of inhibition was reached. Lastly, the light was switched back to λ = 470 nm to ensure levels of original inhibition could be restored. The oocyte was washed for 10 min while **3** was preirradiated. Then the inhibition was tested again with the reverse order of photoswitching. Following 5 min of washing, glycine was reapplied to monitor the reversibility. **B.** Increasing concentrations of λ = 365 and 470 nm irradiated **3** were applied to oocytes expressing GlyT2 to reduce 30 μM glycine transport currents. Transport currents were normalized to the current produced by glycine alone. The closely related GlyT1 transporter was tested at the highest concentration of both isomers of **3** (open circles). **C.** Following inhibition (time 0), oocytes were washed for 5 min, and then glycine was reapplied at 5 min intervals to establish reversibility of each isomer. Shown here is 10 μM inhibition of 300 μM glycine.

Table 1. IC_{50} Values for Inhibition of GlyT2 by (*Z*)-3 and (*E*)-3[a]

	azo-compound **3** IC_{50}	
glycine (μM)	365 nm (*Z*)-**3**	470 nm (*E*)-**3**
10	11.1 (2.37−167) n = 4	4.84 (0.789−26.0) n = 4
30	12.3 (7.81−20.5) n > 4	5.77 (3.18−10.5) n > 4
100	10.6 (4.81−26.5) n = 4	4.49 (2.06−9.55) n = 4
300	9.25 (3.74−26.6) n = 5	7.12 (2.95−18.7) n > 5
1000	6.44 (2.77−15.6) n > 3	4.60 (1.99−10.1) n > 3

[a]Increasing concentrations of (*Z*)-**3** or (*E*)-**3** were applied to oocytes expressing GlyT2 in the presence of 3, 10, 30, 100, 300, and 1000 μM glycine. IC_{50} values for each isomer were calculated at each concentration of glycine and are shown as mean and 95% confidence interval. The IC_{50} values for 3 μM glycine could not be accurately calculated and are omitted from the table.

competitive inhibitors. **3** is therefore unlikely to bind in this region and, rather, may bind in the allosteric site. It is striking that both isomers of **3** inhibit GlyT2, which further suggests that the binding site is a larger, flexible region of the protein.

CONCLUSIONS

In this study, we synthesized azo-compound **3** based on the chemical structures of the GlyT2 inhibitors, ORG25543 (**1**) and compound **2**. Azo-compound **3** was shown to exhibit photocontrolled isomerization and to possess photoswitchable inhibition of GlyT2. Both (*Z*)-**3** and (*E*)-**3** were active, with the *trans* conformation being 2-fold more potent. Despite their differences, it is apparent that both isomers can be accommodated in the binding site, which suggests there is conformational flexibility in this binding region which could inform the design of new inhibitors. We also demonstrate that both conformations of **3** are noncompetitive inhibitors of GlyT2 and are readily reversible, an important consideration when developing GlyT2 targeting inhibitors to treat chronic pain. At this stage the precise location of the binding site for compound **3**, which presumably overlaps with the site for ORG25543, is not well-defined, and further work is required to define specific interactions. This information together with the photoisomerization properties will help to design optimal inhibitors for the control of GlyT2 activity. Furthermore, it is anticipated that a photosensitive GlyT2 inhibitor could be a useful tool for further biological studies focused at identifying the optimal level of GlyT2 inhibition required for treatment of chronic pain conditions. Such compounds may also prove useful in understanding physiological mechanisms of on-target side effects and hyperekplexia-like symptoms. For example, by titrating inhibition at GlyT2 expressing synapses using photoswitching in real-time, the effects on vesicle refilling and recycling could be examined. Future development of photoswitching GlyT2 inhibitors to produce isomers with varying rates of reversibility would be valuable to understand how to produce inhibitors for the treatment of chronic pain while avoiding adverse side effects.

METHODS

Chemistry. *General Chemistry.* All reactions were performed under a dry atmosphere of nitrogen unless otherwise specified. Indicated reaction temperatures refer to the reaction bath, while room temperature (rt) is noted as 25 °C. Commercial grade reagents and anhydrous solvents were used as received from vendors, and no attempts were made to purify or dry these components further. Removal of solvents under reduced pressure was accomplished with a

https://dx.doi.org/10.1021/acschemneuro.9b00655
ACS Chem. Neurosci. 2020, 11, 1250−1258

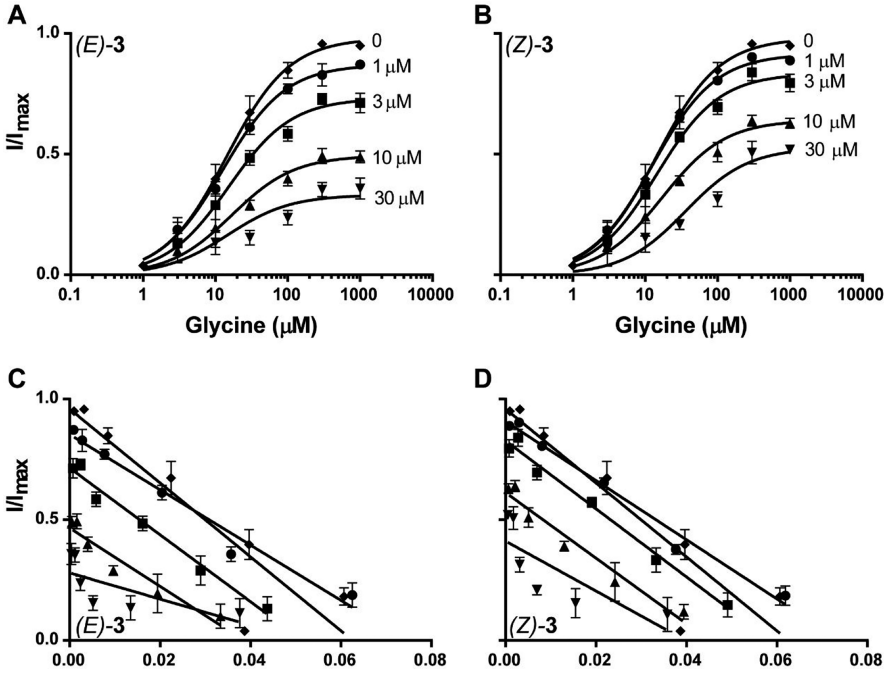

Figure 6. (*Z*)-**3** and (*E*)-**3** reduce concentration-dependent glycine currents. **A.** Concentration-dependent glycine currents were measured in the presence of increasing concentrations of (*Z*)-**3**. **B.** Concentration-dependent glycine currents were measured in the presence of increasing concentrations of (*E*)-**3**. Values shown are means ± SEM. **C and D**. Eadie-Hofstee plots from each indicate both isomers inhibit GlyT2 noncompetitively.

Table 2. EC_{50} and I_{max} Values for Glycine at GlyT2 in the Presence of *cis*- and *trans*-3[a]

	365 nm (*Z*)-**3**		470 nm (*E*)-**3**	
azo-compound **3** (μM)	glycine EC_{50} (μM)	I_{max}	glycine EC_{50} (μM)	I_{max}
0	14.3 ± 1.89 $n > 4$	0.981 ± 0.028	14.3 ± 1.89 $n > 4$	0.981 ± 0.028
1	12.77 ± 1.46 $n > 4$	0.916 ± 0.022	12.7 ± 2.04 $n > 4$	0.872 ± 0.029
3	14.5 ± 2.59 $n > 4$	0.835 ± 0.033	15.3 ± 3.16 $n > 4$	0.732 ± 0.033
10	17.2 ± 3.53 $n > 3$	0.642 ± 0.031	16.8 ± 5.43 $n > 4$	0.495 ± 0.036
30	36.0 ± 17.5 $n > 3$	0.527 ± 0.063	14.8 ± 8.57 $n > 3$	0.332 ± 0.043

[a]Glycine concentration-dependent currents were measured in the presence of **3** and fit to the Michaelis–Menten equation to calculate EC_{50} values which are shown as mean ± SEM. I_{max} values were normalized to the I_{max} of glycine transport in the absence of inhibitor and are shown as mean ± SEM.

Buchi rotary evaporator at approximately 28 mmHg pressure using a Teflon-linked KNF vacuum pump. Thin layer chromatography was performed using 1″ × 3″ AnalTech No. 02521 silica gel plates with a fluorescent indicator. Visualization of TLC plates was made by observation with either short wave UV light (254 nm lamp), 10% phosphomolybdic acid in ethanol, or in iodine vapors. Preparative thin layer chromatography was performed using Analtech, 20 × 20 cm, 1000 μm preparative TLC plates. Flash column chromatography was carried out using a Teledyne Isco CombiFlash Companion Unit with RediSep Rf silica gel columns. Proton NMR spectra were obtained on a 400 MHz Varian Nuclear Magnetic Resonance Spectrometer, chemical shifts (δ) are reported in parts per million (ppm), and coupling constant (J) values are given in Hz, with the following spectral pattern designations: s, singlet; d, doublet; t, triplet, q, quartet; dd, doublet of doublets; m, multiplet; br, broad. Tetramethylsilane was used as an internal reference. Mass spectroscopic analyses were performed using ESI ionization on a Waters AQUITY UPLC MS single quadrapole mass spectrometer. High pressure liquid chromatography (HPLC) purity analysis was performed using a Waters Breeze2 HPLC system with a binary solvent system A and B using a gradient elusion [A, H_2O with 0.25% TFA; B, CH_3CN with 0.25% TFA] and flow rate = 1 mL/min, with UV detection at 254 nm (system equipped with a photodiode array (PDA) detector). The purity of all tested compounds was >95% as confirmed by reverse phase analytical HPLC and ^1H NMR.

*(E)-N-((1-(Dimethylamino)cyclohexyl)methyl)-3-methoxy-4-(phenyldiazenyl)benzamide ((E)-**3**) and (Z)-N-((1-(Dimethylamino)-cyclohexyl)methyl)-3-methoxy-4-(phenyldiazenyl)benzamide ((Z)-**3**).* Step A: To a 0 °C cooled solution of cyclohexanone (**4**, 5.0 g, 50.0 mmol) in H_2O (50 mL) was added dimethylamine hydrochloride (4.10 g, 50.0 mmol) and KCN (3.30 g, 50.0 mmol). The resultant mixture stirred for 18 h while gradually warming to rt. The mixture was diluted with additional H_2O (100 mL) and then extracted with Et_2O (3 × 100 mL). The combined organic extracts were washed with brine, dried over Na_2SO_4, filtered, and concentrated under reduced pressure to give 1-(dimethylamino)cyclohexane-1-carbonitrile (**5**, 8.0 g crude): ESI MS m/z = 153 $[M + H]^+$.

Step B: To a 0 °C cooled solution of 1-(dimethylamino)-cyclohexane-1-carbonitrile (**5**, 7.5 g, 49.0 mmol) in Et_2O (50 mL) was added $LiAlH_4$ (2.40 g, 64.0 mmol) portionwise. The resultant mixture stirred for 18 h while gradually warming to rt under an atmosphere of N_2. The mixture was then cooled back to 0 °C, carefully quenched with aqueous 2 M NaOH (3 mL), and filtered through a pad of Celite. The aqueous filtrate was extracted with Et_2O (3 × 100 mL), and the combined organic extracts were dried over Na_2SO_4 and filtered. Due to the high volatility of 1-(aminomethyl)-*N*,*N*-dimethylcyclohexan-1-amine (**6**), the resulting solution contain-

https://dx.doi.org/10.1021/acschemneuro.9b00655
ACS Chem. Neurosci. 2020, 11, 1250−1258

ing the crude product in Et_2O was not concentrated under reduced pressure and was instead used as is in the next step with an estimated concentration of 7.6 g of **6** (theoretical yield) in 100 mL of Et_2O (~0.49 M): ESI MS m/z = 157 $[M + H]^+$.

Step C: A mixture of methyl 4-amino-3-methoxybenzoate (**7**, 1.0 g, 5.52 mmol) and nitrosobenzene (0.77 g, 7.18 mmol) in HOAc (15 mL) was heated at 40 °C for 16 h. The reaction was allowed to cool to rt, then carefully quenched with H_2O (200 mL), and neutralized to pH = 7 with aqueous saturated $NaHCO_3$ solution (5 mL). The aqueous mixture was extracted with EtOAc (3 × 100 mL). The aqueous mixture was extracted with EtOAc (3 × 20 mL), and the combined organic extracts were washed with brine, dried over anhydrous Na_2SO_4, and concentrated under reduced pressure. The resulting residue was chromatographed over silica gel (Isco CombiFlash Companion unit, 12 g Redisep column, 0−30% EtOAc in hexanes) to give methyl (*E*)-3-methoxy-4-(phenyldiazenyl)-benzoate ((*E*)-**8**) as an orange solid (1.4 g, 94%): ^{1}H NMR (400 MHz, DMSO-d_6) δ 7.84−7.82 (m, 2 H), 7.69 (s, 1H), 7.61−7.51 (m, 5 H), 3.97 (s, 3 H), 3.85 (s, 3 H); ESI MS m/z = 271 $[M + H]^+$.

Step D: To a solution of methyl (*E*)-3-methoxy-4-(phenyldiazenyl)benzoate ((*E*)-**8**, 1.4 g, 5.19 mmol) in a 1:4 mixture of THF (10 mL) and CH_3OH (40 mL) was added aqueous 2 N NaOH (13 mL, 26.00 mmol). The mixture stirred for 16 h at rt. The mixture was concentrated under reduced pressure, and the crude residue was diluted with H_2O (50 mL) and neutralized to pH = 7 with aqueous 2 N HCl. The aqueous mixture was extracted with EtOAc (3 × 20 mL), and the combined organic extracts were washed with brine, dried over anhydrous $MgSO_4$, and concentrated under reduced pressure to give (*E*)-3-methoxy-4-(phenyldiazenyl)benzoic acid ((*E*)-**9**) as an orange solid (680 mg, 52% yield): ^{1}H NMR (400 MHz, DMSO-d_6) δ 7.84−7.82 (m, 2 H), 7.70 (s, 1H), 7.61−7.50 (m, 5 H), 3.97 (s, 3 H); ESI MS m/z = 257 $[M + H]^+$.

Step E: To a solution of (*E*)-3-methoxy-4-(phenyldiazenyl)benzoic acid ((*E*)-**9**, 0.20 g, 0.78 mmol), HBTU (0.44 g, 1.17 mmol), and *i*-Pr_2NEt (0.40 mL, 2.34 mmol) in THF (16 mL) was added an ~0.49 M solution of 1-(aminomethyl)-*N*,*N*-dimethylcyclohexan-1-amine in Et_2O (**6**, 15.9 mL, 7.81 mmol). The mixture stirred at rt for 18 h under an atmosphere of N_2. The mixture was concentrated under reduced pressure, and the resulting residue was chromatographed over silica gel (Isco CombiFlash Companion unit, 12 g Redisep column, 0−10% CH_3OH in CH_2Cl_2) to afford a mixture of isomers (*E*)-*N*-((1-(dimethylamino)cyclohexyl)methyl)-3-methoxy-4-(phenyldiazenyl)benzamide ((*E*)-**3**) and (*Z*)-*N*-((1-(dimethylamino)cyclohexyl)methyl)-3-methoxy-4-(phenyldiazenyl)-benzamide ((*Z*)-**3**) as an orange solid (121.0 mg, 40%). The individual geometric isomers (*E*)-**3** and (*Z*)-**3** readily interconverted and could not be isolated separately and independently characterized. The HPLC and ^{1}H NMR data generated indicates a nearly 1:1 mixture of (*E*)-**3** and (*Z*)-**3**: ^{1}H NMR (400 MHz, DMSO-d_6): δ 8.76−7.82 (m, 3 H), 8.42 (brs, 1 H), 8.11 (brs, 1 H), 7.83 (d, J = 5.6 Hz, 2 H), 7.66 (s, 1H), 7.57−7.56 (m, 4 H), 7.35−7.12 (m, 3 H), 6.81 (d, J = 7.6 Hz, 1 H), 6.74 (d, J = 8.4 Hz, 1 H), 3.99 (s, 3 H), 3.61−3.53 (m, 2 H), 3.12−3.06 (m, 2 H), 2.80−2.79 (m, 6 H), 2.75−2.74 (m, 3 H), 1.64−1.54 (m, 10 H); ESI MS m/z = 395 $[M + H]^+$; HPLC 99.76% total purity (AUC), peak 1 t_R = 12.06 min (42.57%), peak 2 t_R = 12.79 min (57.19%).

UV−Visible Spectroscopy. Isomerization of azo-compound **3** was monitored using a Cary 60 v2.0 UV−visible spectrophotometer (Agilent). A solution of azo-compound **3** was made in phosphate-buffered saline (PBS; pH 7.4) to a final concentration of 20 ppm (20 μg/mL). An initial baseline absorbance of this solution was determined at time, t = 0. The azo-compound **3** solution was irradiated with λ = 470 nm blue light using an external light source (pE200-CooLED) at an intensity of 0.02 mW/cm^2 for 15 min to ensure that the entire solution was in the *trans* configuration; the corresponding absorbance was determined. Subsequently, the azo-compound **3** solution was irradiated with λ = 365 nm UV-A light using the same light source at the same intensity in 5 s intervals, and the corresponding absorbance was simultaneously determined using a start (800 nm)/stop (200 nm) measurement protocol (scan rate = 24000 nm/min; data interval = 5 nm; average time = 0.0125 s) until no further change in absorbance was observed, i.e., the *trans* isomer was completely isomerized to the *cis* isomer. The azo-compound **3** solution was then irradiated with λ = 470 nm blue light using the same light source at the same intensity in 5 s intervals, and the corresponding absorbance was simultaneously determined using the same protocol until no further change in absorbance was observed.

For the thermal relaxation study, a solution of **3** in a well-sealed cuvette was irradiated with 365 nm UV light for 5 min. The resulting solution of (*Z*)-**3** was then placed in a Cary 60 v2.0 UV−visible spectrophotometer that was set to record UV−vis spectra at 12 h time intervals. The solution was left in the dark until no further changes in the UV/vis spectra were observed.

Electrophysiology. Human GlyT2a DNA subcloned into the plasmid oocyte transcription vector was linearized with SpeI (New England Biolabs (Genesearch), Arundel, Australia), and RNA was transcribed using T7 RNA polymerase (mMessage mMachine kit, Ambion, TX). RNA encoding the transporter was then injected into defoliculated *Xenopus laevis* oocytes with a Drummond Nanoinject (Drummond Scientific Co., Broomall, PA). The oocytes were then stored at 16−18 °C for 2−5 days in ND96 solution (96 mM NaCl, 2 mM KCL,1 mM MgCl2, 1.8 mM CaCl2, 5 mM HEPES, pH 7.55), supplemented with 2.5 mM sodium pyruvate, 0.5 mM theophylline, 50 μg/mL gentamicin, and 100 μM/mL tetracycline, until transporter expression was sufficient to measure transport currents.

Oocytes were held at −60 mV, and glycine transport currents were measured using a Geneclamp 500 amplifier (Axon Instruments, Foster City, CA) with a Powerlab 2/20 chart recorder (ADInstruments, Sydney, Australia), interfaced with chart software (ADInstruments). Isomerization was achieved using an external light source (pE200-CooLED) with a liquid light guide directed over the recording solution to maximize the intensity of light incident. All experiments were carried out in a dark, enclosed, Faraday cage to minimize background interference.

Increasing concentrations of azo-compound **3** (1, 3, 10, 30 μM) were coapplied to oocytes in the presence of a range of glycine concentrations (3, 10, 30, 100, 1000, 3000 μM). At each concentration, the light source was switched from 470 to 365 nm and then 365 to 470 nm, to generate plateau values of inhibition that were distinct for each isomer. Following inhibition, glycine was reapplied to determine the reversibility of azo-compound **3**. Currents were normalized to the maximal current produced by glycine in the absence of any inhibitor. Data were analyzed using GraphPad Prism 7.02 (GraphPad Software, San Diego, CA). Glycine concentration responses were fit to the Michaelis−Menten equation, I = ([Gly] I_{max})/EC_{50} + [Gly], and then transformed using an Eadie-Hofstee plot. Inhibitor concentration responses were fit by the method of least-squares using Y = bottom + (top−bottom)/(1 + 10(X − log IC_{50})), where X is log[azo-compound **3**] (μM), Y is the current normalized to glycine in the absence of inhibitor, and top and bottom are the maximal and minimal plateau responses, respectively.

AUTHOR INFORMATION

Corresponding Author

Robert J. Vandenberg − *Discipline of Pharmacology, School of Medical Sciences, Faculty of Medicine and Health, University of Sydney, Camperdown, New South Wales 2006, Australia;* orcid.org/0000-0003-1523-4814; Email: robert.vandenberg@sydney.edu.au

Authors

Shannon N. Mostyn − *Discipline of Pharmacology, School of Medical Sciences, Faculty of Medicine and Health, University of Sydney, Camperdown, New South Wales 2006, Australia*

Subhodeep Sarker − *Discipline of Pharmacology, School of Medical Sciences, Faculty of Medicine and Health, University of Sydney, Camperdown, New South Wales 2006, Australia*

https://dx.doi.org/10.1021/acschemneuro.9b00655
ACS Chem. Neurosci. 2020, 11, 1250−1258

Parthasarathy Muthuraman − *Basic and Clinical Sciences and Pharmaceutical Sciences, Albany College of Pharmacy and Health Sciences, Albany, New York 12208, United States*
Arun Raja − *Basic and Clinical Sciences and Pharmaceutical Sciences, Albany College of Pharmacy and Health Sciences, Albany, New York 12208, United States*
Susan Shimmon − *School of Mathematical and Physical Sciences, University of Technology Sydney, Ultimo, New South Wales 2007, Australia*
Tristan Rawling − *School of Mathematical and Physical Sciences, University of Technology Sydney, Ultimo, New South Wales 2007, Australia;* orcid.org/0000-0002-6624-6586
Christopher L. Cioffi − *Basic and Clinical Sciences and Pharmaceutical Sciences, Albany College of Pharmacy and Health Sciences, Albany, New York 12208, United States;* orcid.org/0000-0003-0642-7905

Complete contact information is available at: https://pubs.acs.org/10.1021/acschemneuro.9b00655

Author Contributions

‖S.N.M. and Su.Sa. contributed equally.

Author Contributions

S.N.M. and Su.Sa. designed and conducted experiments with GlyT2 expressing *Xenopus laevis* oocytes, analyzed data, and wrote the manuscript. P.M., A.R., and C.C. designed and synthesized compounds. Su.Sh. and T.R. characterized the photoswitchable properties of the compound. R.J.V. helped design the study, analyzed data. and wrote the manuscript. R.J.V., C.C., and Su.Sa. obtained funding to support the work.

Funding

This work was supported by the Australian National Health and Medical Research Council (NHMRC) Project Grant APP1144429. Su.Sa. was supported by the Austrian Science Fund (FWF) Erwin-Schrödinger-Fellowship Program Project No. J3982-B27.

Notes

The authors declare no competing financial interest.

■ ACKNOWLEDGMENTS

We thank Jamie Vandenberg, Mathew Perry, and Chai-Ann Ng for advice and use of the pE200-CooLED light source and Cheryl Handford for maintaining the *Xenopus laevis* facility.

■ ABBREVIATIONS

GlyT2, glycine transporter 2; THF, tetrahydrofuran; Et_2O, diethyl ether; EtOAc, ethyl acetate; CH_3OH, methyl alcohol; *i*-Pr_2NEt, *N*,*N*-diisopropylethylamine; NaOH, sodium hydroxide; $LiAlH_4$, lithium aluminum hydride; CH_2Cl_2, dichloromethane; rt, room temperature; KCN, potassium cyanide; HBTU, (2-(1*H*-benzotriazol-1-yl)-1,1,3,3-tetramethyluronium hexafluorophosphate; HOAc, acetic acid; 10% Pd/C, 10% palladium on carbon (wet, wt/wt); CH_3I, methyl iodide; K_2CO_3, potassium carbonate; CH_3CN, acetonitrile; TFA, trifluoroacetic acid

■ REFERENCES

(1) Latremoliere, A., and Woolf, C. J. (2009) Central sensitization: a generator of pain hypersensitivity by central neural plasticity. *J. Pain 10* (9), 895−926.
(2) Takazawa, T., and MacDermott, A. B. (2010) Synaptic pathways and inhibitory gates in the spinal cord dorsal horn. *Ann. N. Y. Acad. Sci. 1198*, 153−8.
(3) Todd, A. J. (2010) Neuronal circuitry for pain processing in the dorsal horn. *Nat. Rev. Neurosci. 11* (12), 823−36.
(4) Imlach, W. L., Bhola, R. F., Mohammadi, S. A., and Christie, M. J. (2016) Glycinergic dysfunction in a subpopulation of dorsal horn interneurons in a rat model of neuropathic pain. *Sci. Rep. 6*, 37104.
(5) Eulenburg, V., Armsen, W., Betz, H., and Gomeza, J. (2005) Glycine transporters: essential regulators of neurotransmission. *Trends Biochem. Sci. 30* (6), 325−33.
(6) Dohi, T., Morita, K., Kitayama, T., Motoyama, N., and Morioka, N. (2009) Glycine transporter inhibitors as a novel drug discovery strategy for neuropathic pain. *Pharmacol. Ther. 123* (1), 54−79.
(7) Vandenberg, R. J., Ryan, R. M., Carland, J. E., Imlach, W. L., and Christie, M. J. (2014) Glycine transport inhibitors for the treatment of pain. *Trends Pharmacol. Sci. 35* (8), 423−430.
(8) Vandenberg, R. J., Mostyn, S. N., Carland, J. E., and Ryan, R. M. (2016) Glycine transporter 2 inhibitors: Getting the balance right. *Neurochem. Int. 98*, 89−93.
(9) Cioffi, C. L. (2018) Modulation of glycine-mediated spinal neurotransmission for the treatment of chronic pain. *J. Med. Chem. 61*, 2652−2679.
(10) Morita, K., Motoyama, N., Kitayama, T., Morioka, N., Kifune, K., and Dohi, T. (2008) Spinal antiallodynia action of glycine transporter inhibitors in neuropathic pain models in mice. *J. Pharmacol. Exp. Ther. 326* (2), 633−45.
(11) Gomeza, J., Ohno, K., Hulsmann, S., Armsen, W., Eulenburg, V., Richter, D. W., Laube, B., and Betz, H. (2003) Deletion of the mouse glycine transporter 2 results in a hyperekplexia phenotype and postnatal lethality. *Neuron 40* (4), 797−806.
(12) Eulenburg, V., Becker, K., Gomeza, J., Schmitt, B., Becker, C. M., and Betz, H. (2006) Mutations within the human GLYT2 (SLC6A5) gene associated with hyperekplexia. *Biochem. Biophys. Res. Commun. 348* (2), 400−5.
(13) Carta, E., Chung, S. K., James, V. M., Robinson, A., Gill, J. L., Remy, N., Vanbellinghen, J. F., Drew, C. J., Cagdas, S., Cameron, D., Cowan, F. M., Del Toro, M., Graham, G. E., Manzur, A. Y., Masri, A., Rivera, S., Scalais, E., Shiang, R., Sinclair, K., Stuart, C. A., Tijssen, M. A., Wise, G., Zuberi, S. M., Harvey, K., Pearce, B. R., Topf, M., Thomas, R. H., Supplisson, S., Rees, M. I., and Harvey, R. J. (2012) Mutations in the GlyT2 gene (SLC6A5) are a second major cause of startle disease. *J. Biol. Chem. 287* (34), 28975−85.
(14) Rees, M. I., Harvey, K., Pearce, B. R., Chung, S. K., Duguid, I. C., Thomas, P., Beatty, S., Graham, G. E., Armstrong, L., Shiang, R., Abbott, K. J., Zuberi, S. M., Stephenson, J. B., Owen, M. J., Tijssen, M. A., van den Maagdenberg, A. M., Smart, T. G., Supplisson, S., and Harvey, R. J. (2006) Mutations in the gene encoding GlyT2 (SLC6A5) define a presynaptic component of human startle disease. *Nat. Genet. 38* (7), 801−6.
(15) Caulfield, W. L., Collie, I. T., Dickins, R. S., Epemolu, O., McGuire, R., Hill, D. R., McVey, G., Morphy, J. R., Rankovic, Z., and Sundaram, H. (2001) The first potent and selective inhibitors of the glycine transporter type 2. *J. Med. Chem. 44* (17), 2679−82.
(16) Mingorance-Le Meur, A., Ghisdal, P., Mullier, B., De Ron, P., Downey, P., Van Der Perren, C., Declercq, V., Cornelis, S., Famelart, M., Van Asperen, J., Jnoff, E., and Courade, J. P. (2013) Reversible inhibition of the glycine transporter GlyT2 circumvents acute toxicity while preserving efficacy in the treatment of pain. *Br. J. Pharmacol. 170* (5), 1053−63.
(17) Mostyn, S. N., Rawling, T., Mohammadi, S., Shimmon, S., Frangos, Z. J., Sarker, S., Yousuf, A., Vetter, I., Ryan, R. M., Christie, M. J., and Vandenberg, R. J. (2019) Development of an N-acyl amino acid that selectively inhibits the glycine transporter 2 to produce analgesia in a rat model of chronic pain. *J. Med. Chem. 62* (5), 2466−2484.
(18) Bradaia, A., Schlichter, R., and Trouslard, J. (2004) Role of glial and neuronal glycine transporters in the control of glycinergic and glutamatergic synaptic transmission in lamina X of the rat spinal cord. *J. Physiol. 559* (Pt1), 169−186.

(19) Lerch, M. M., Hansen, M. J., van Dam, G. M., Szymanski, W., and Feringa, B. L. (2016) Emerging Targets in Photopharmacology. *Angew. Chem., Int. Ed. 55* (37), 10978−99.
(20) Ankenbruck, N., Courtney, T., Naro, Y., and Deiters, A. (2018) Optochemical Control of Biological Processes in Cells and Animals. *Angew. Chem., Int. Ed. 57* (11), 2768−2798.
(21) Bandara, H. M., and Burdette, S. C. (2012) Photoisomerization in different classes of azobenzene. *Chem. Soc. Rev. 41* (5), 1809−25.
(22) Quandt, G., Hofner, G., Pabel, J., Dine, J., Eder, M., and Wanner, K. T. (2014) First photoswitchable neurotransmitter transporter inhibitor: light-induced control of gamma-aminobutyric acid transporter 1 (GAT1) activity in mouse brain. *J. Med. Chem. 57* (15), 6809−21.
(23) Frank, J. A., Moroni, M., Moshourab, R., Sumser, M., Lewin, G. R., and Trauner, D. (2015) Photoswitchable fatty acids enable optical control of TRPV1. *Nat. Commun. 6*, 7118.
(24) Cheng, B., Shchepakin, D., Kavanaugh, M. P., and Trauner, D. (2017) Photoswitchable Inhibitor of a Glutamate Transporter. *ACS Chem. Neurosci. 8* (8), 1668−1672.
(25) Morstein, J., Awale, M., Reymond, J.-L., and Trauner, D. (2019) Mapping the Azolog Space Enables the Optical Control of New Biological Targets. *ACS Cent. Sci. 5*, 607−618.
(26) Brameld, K. A., Kuhn, B., Reuter, D. C., and Stahl, M. (2008) Small molecule conformational preferences derived from crystal structure data. A medicinal chemistry focused analysis. *J. Chem. Inf. Model. 48* (1), 1−24.
(27) Chein, R. J., and Corey, E. J. (2010) Strong conformational preferences of heteroaromatic ethers and electron pair repulsion. *Org. Lett. 12* (1), 132−5.
(28) Kyziol, J. B., and Frej, H. (1988) Substituent effects on physical properties of substituted azobenzenes. *Chemical Papers 42* (6), 781−793.
(29) Coleman, J. A., Green, E. M., and Gouaux, E. (2016) X-ray structures and mechanism of the human serotonin transporter. *Nature 532* (7599), 334−9.
(30) Carland, J. E., Thomas, M., Mostyn, S. N., Subramanian, N., O'Mara, M. L., Ryan, R. M., and Vandenberg, R. J. (2018) Molecular Determinants for Substrate Interactions with the Glycine Transporter GlyT2. *ACS Chem. Neurosci. 9* (3), 603−614.

https://dx.doi.org/10.1021/acschemneuro.9b00655
ACS Chem. Neurosci. 2020, 11, 1250−1258